Hong, K.-C., et al., 2024, Oligocene melting of subducted mélange and its mantle dynamics in northeast Asia: Geology, https://doi.org/10.1130/G52115.1

Supplemental Material

Detailed analytical methods, Tables S1–S4, and Figures S1–S4.

Oligocene melting of subducted mélange and its mantle dynamics in northeast Asia

Ke-Chun Hong[1], Feng Wang[1, 2*], Si-Wen Zhang[1], Wen-Liang Xu[1, 2], Yi-Ni Wang[1, 2], and De-Bin Yang[1, 2]

[1]*College of Earth Sciences, Jilin University, Changchun 130061, China*

[2]*Key Laboratory of Mineral Resources Evaluation in Northeast Asia, Ministry of Natural Resources, Changchun 130061, China*

Supplemental Material

Analytical methods, supplementary figures, tables and references

Analytical methods

1. Analytical methods of zircon U-Pb dating

Zircons were separated from whole-rock samples using the conventional heavy liquid and magnetic techniques, and then by handpicking under a binocular microscope, at the Langfang Regional Geological Survey, Hebei Province, China. The handpicked zircons were examined under transmitted and reflected light with an optical microscope. To reveal their internal structures, cathodoluminescence (CL) images were obtained using a JEOL scanning electron microscope housed at the State Key Laboratory of Geological Processes and Mineral Resources, China University of Geosciences, Wuhan, China. Distinct domains within the zircons were selected for analysis, based on the CL images. Two methods such as secondary ion mass spectrometry (SIMS) and laserablation inductively coupled plasma mass spectrometry (LA-ICP-MS) are used for zircon U–Pb dating.

SIMS zircon U–Pb analyses were conducted using the CAMECA IMS1280 ion microprobe at the Institute of Geology and Geophysics, Chinese Academy of Sciences, Beijing, China. U-Th-Pb ratios and absolute abundance were determined relative to the standard zircon 91500 (Wiedenbeck et al., 1995), analyses of which were interspersed with those of unknown grains, using operating and data processing procedures similar to those described by Li et al. (2009). The mass resolution used to measure U–Pb isotopes was 5400 during the analytical session. Isotopic compositions were corrected for common Pb using the measured ^{204}Pb. Corrections were sufficiently small to be insensitive to the choice of common-Pb composition, and an average of presentday crustal composition (Stacey and Kramers, 1975) was used, assuming that the common Pb is largely from surface contamination or from the gold coating introduced during sample preparation. Uncertainties on individual analyses in data tables are reported at the 1σ

level; mean ages for pooled U/Pb analyses are quoted at the 95% confidence interval. Data reduction was performed using the Isoplot/Ex v. 3.0 (Ludwig, 2003).

LA-ICP-MS zircon U–Pb analyses were performed using an Agilent 7500a ICP-MS equipped with a 193 nm laser, housed at the State Key Laboratory of Geological Processes and Mineral Resources, China University of Geosciences, Wuhan, China. The zircon 91500 was used as an external standard for age calibration, and the NIST SRM 610 silicate glass was applied for instrument optimization. The crater diameter was 32 μm during the analyses. The instrument parameter and detail procedures were described by Yuan et al. (2004). The ICPMSDataCal (Ver. 6.7; Liu et al., 2008; Liu et al., 2010) and Isoplot (Ver. 3.0; Ludwig, 2003) programs were used for data reduction. Correction for common Pb was made following Anderson (2002). Errors in individual analyses by LA-ICP-MS are quoted at the 1σ level, while errors in pooled ages are quoted at the 95% (2σ) confidence level. The dating results are presented in Table S1.

2. Analytical methods of whole-rock major and trace element determinations

The sample pretreatment of whole rock for major element analysis was made by the melting method. The flux is a mixture of lithium tetraborate, lithium metaborate, and lithium fluoride (45:10:5). Ammonium nitrate and lithium bromide were used as oxidants and release agents, respectively. The melting temperature was 1050 ℃ and the melting time was 15 minutes.

Zsx Primus II wavelength dispersive X-ray fluorescence spectrometer (XRF) produced by RIGAKU, Japan was used for the analysis of major elements in the whole rock. The X-ray tube is a 4.0 Kw end window Rh target. The test conditions are voltage: 50 kV, current: 60mA, and all major element analysis lines are kα. The standard curve uses the national standard material: rock standard sample GBW07101-14. The data were corrected by the theoretical α coefficient method. The relative standard deviation (RSD) is less than 2%.

Trace element analysis of whole rocks was conducted on an Agilent 7700e ICP-MS at the Wuhan Sample Solution Analytical Technology Co., Ltd., Wuhan, China. The detailed sample-digesting procedure was as follows: (1) Sample powder (200 mesh) were placed in an oven at 105 ℃ for drying of 12 hours; (2) 50 mg sample powder was accurately weighed and placed in a Teflon bomb; (3) 1 mL HNO_3 and 1 mL HF were slowly added into the Teflon bomb; (4) Teflon bomb was putted in a stainless steel pressure jacket and heated to 190 ℃ in an oven for >24 hours; (5) After cooling, the Teflon bomb was opened and placed on a hotplate at 140 ℃ and evaporated to incipient dryness, and then 1 mL HNO_3 was added and evaporated to dryness again; (6) 1 mL of HNO_3, 1 mL of MQ water and 1 mL internal standard solution of 1ppm In were added, and the Teflon bomb was resealed and placed in the oven at 190 ℃ for >12 hours; (7) The final solution was transferred to a polyethylene bottle and diluted to 100 g by the addition of 2% HNO_3.

3. Analytical methods of Sr-Nd isotopes

Whole-rock Sr–Nd isotope data were measured on Wuhan Shangpu Solution Analytical Technology Co., Ltd. All chemical preparations were performed on class 100 work benches within a class 1000 overpressured clean laboratory.

Sample digestion: (1) Sample powder (200 mesh) was placed in an oven at 105 ℃ for drying of 12 hours; (2) 50-200 mg sample powder was accurately weighed and placed in a Teflon bomb; (3) 1-3 mL HNO_3 and 1-3 mL HF were added into the Teflon bomb; (4) the Teflon bomb was putted in a stainless steel pressure jacket and heated to 190 ℃ in an oven for >24 hours; (5) After cooling, the Teflon bomb was opened and placed on a hotplate at 140 ℃ and evaporated to incipient dryness, and then 1 mL HNO_3 was added and evaporated to dryness again; (6) The sample was dissolved in 1.0 mL of 2.5 M HCl.

Column chemistry: After centrifugation, the supernatant solution was loaded into an ion-exchange column packed with AG50W resin. After complete draining of the sample solution, columns were rinsed with 20 mL of 2.5 M HCl to remove undesirable matrix elements. Finally, the Sr fraction was eluted using 10 mL of 2.5 M HCl and gently evaporated to dryness prior to mass-spectrometric measurement. The residue was rinsed with 10 mL of 4.0 M HCl, and then the REE fraction was eluted using 10 mL of 4.0 M HCl. The REE solution was used to separate the Nd fraction by the Nd-column method.

The Sr fraction was separated again by the Sr-specific resin. The solution was first converted to the HNO_3 medium (3 M HNO_3). Then the solution was loaded into the Sr-specific resin (SR-B50-S) and pre-conditioned with 6 M HCl and 3 M HNO_3. After complete draining of the sample solution, columns were rinsed with 3 M HNO_3 to remove undesirable matrix elements. Finally, Sr was eluted using MQ H_2O and gently evaporated to dryness prior to mass spectrometric measurement. The REE solution was evaporated to incipient dryness and taken up with 0.18 M HCl. The converted REE solution was loaded into an ion-exchange column packed with LN resin. After complete draining of the sample solution, columns were rinsed with 18mL of 0.18 M HCl to remove undesirable matrix elements. Finally, the Nd fraction was eluted using 5mL of 0.3 M HCl and gently evaporated to dryness prior to mass spectrometric measurement.

Sr isotope analyses were performed on a Neptune Plus MC-ICP-MS (Thermo Fisher Scientific, Dreieich, Germany). The Neptune Plus, a double focusing MC-ICP-MS, was equipped with seven fixed electron multiplier ICs, and nine Faraday cups fitted with 10^{11} Ω resistors. The faraday collector configuration of the mass system was composed of an array from L4 to H3 to monitor $^{83}Kr^{+}$, $^{167}Er^{++}$, $^{84}Sr^{+}$, $^{85}Rb^{+}$, $^{86}Sr^{+}$, $^{173}Yb^{++}$, $^{87}Sr^{+}$ and $^{88}Sr^{+}$. The large dry interface pump (120 m^3 hr^{-1} pumping speed), the newly designed H skimmer cone and the

standard sample cone were used to increase the instrumental sensitivity. Sr single element solution from Alfa (Alfa Aesar, Karlsruhe, Germany) was used to optimize instrument operating parameters. An aliquot of the international standard solution of 200 μg/L NIST SRM 987 was regularly used for evaluating the reproducibility and accuracy of the instrument. Typically, the signal intensities of ^{88}Sr in NIST 987 were > ~7.0 V. The Sr isotopic data were acquired in the static mode at low resolution. The routine data acquisition consisted of ten blocks of 10 cycles (4.194 s integration time per cycle). The total time of one measurement lasted about 7 minutes.

The exponential law, which was initially developed for TIMS measurement (Russell et al. 1978) and remains the most widely accepted and utilized with MC-ICP-MS, was used to assess the instrumental mass discrimination in this study. Mass discrimination correction was carried out via internal normalization to a $^{88}Sr/^{86}Sr$ ratio of 8.375209 (Lin et al. 2016). The interference elements Ca, Rb, Er, and Yb have been completely separated by the exchange resin process. The remaining interferences of $^{83}Kr^{+}$, $^{85}Rb^{+}$, $^{167}Er^{++}$ and $^{173}Yb^{++}$ were corrected based on the methed described by Lin et al. (2016). One international NIST 987 standard was measured for every seven samples analyzed. All data reduction for the MC-ICP-MS analysis of Sr isotope ratios was conducted using "Iso-Compass" software (Zhang et al. 2020). Analyses of the NIST 987 standard solution yielded an $^{87}Sr/^{86}Sr$ ratio of 0.710243 ± 8 (2SD), which is identical within error to their published values 0.710241 ± 12 (Thirlwall, 1991). In addition, the reference materials BCR-2 (basalt) and RGM-2 (rhyolite) yielded results of 0.705009 ± 8 (2SD) and 0.704152 ± 8 (2SD) for $^{87}Sr/^{86}Sr$, respectively, which are identical within error to their published values (Li et al., 2012).

Nd isotope analyses were performed on a Neptune Plus MC-ICP-MS (Thermo Fisher Scientific, Dreieich, Germany). The Neptune Plus, a double focusing MC-ICP-MS, was

equipped with seven fixed electron multiplier ICs and nine Faraday cups fitted with 10^{11} Ω resistors. The faraday collector configuration of the mass system was composed of an array from L4 to H4 to monitor $^{142}Nd^{+}$, $^{143}Nd^{+}$, $^{144}Nd^{+}$, $^{145}Nd^{+}$, $^{146}Nd^{+}$, $^{147}Sm^{+}$, $^{148}Nd^{+}$, $^{149}Sm^{+}$ and $^{150}Nd^{+}$. The large dry interface pump (120 m^3 hr^{-1} pumping speed), the newly designed H skimmer cone, and the standard sample cone were used to increase the instrumental sensitivity. Nd single element solution from Alfa (Alfa Aesar, Karlsruhe, Germany) was used to optimize instrument operating parameters. An aliquot of the standard solution of 200 μg/L GSB 04-3258-2015 was regularly used for evaluating the reproducibility and accuracy of the instrument. Typically, the signal intensities of $^{142}Nd^{+}$ in GSB 04-3258-2015 were > ~2.5 V. The Nd isotopic data were acquired in the static mode at low resolution. The routine data acquisition consisted of ten blocks of 10 cycles (4.194 s of integration time per cycle). The total time of one measurement lasted about 7 minutes.

The exponential law, which was initially developed for TIMS measurement (Russell et al. 1978) and remains the most widely accepted and utilized with MC-ICP-MS, was used to assess the instrumental mass discrimination in this study. Mass discrimination correction was carried out via internal normalization to a $^{146}Nd/^{144}Nd$ ratio of 0.7219 (Lin et al. 2016). The interference elements Sm have been completely separated by the exchange resin process. The remaining interferences of $^{144}Sm+$ were corrected based on the methed described by Lin et al. (2016). All data reduction for the MC-ICP-MS analysis of Nd isotope ratios was conducted using "Iso-Compass" software (Zhang et al. 2020). One GSB 04-3258-2015 standard was measured for every seven samples analyzed. Analyses of the GSB 04-3258-2015 standard yielded $^{143}Nd/^{144}Nd$ ratio of 0.512441 ±8 (2SD), which is identical within error to their published values (0.512438 ± 6 (2SD); Li et al., 2017). In addition, the USGS reference materials BCR-2 (basalt) and RGM-2

(rhyolite) yielded results of 0.512647 ± 6 (2SD) and 0.512807 ± 8 (2SD) for $^{143}Nd/^{144}Nd$, respectively, which is identical within error to their published values (Weis at al., 2006; Li et al. 2012).

4. Analytical methods of Pb isotope

Whole-rock Pb isotope data were measured on Wuhan Shangpu Solution Analytical Technology Co., Ltd. All chemical preparations were performed on class 100 work benches within a class 1000 overpressured clean laboratory.

Sample digestion: (1) Sample powder (200 mesh) was placed in an oven at 105 ℃ for drying of 12 hours; (2) 50-200 mg sample powder was accurately weighed and placed in a Teflon bomb; (3) 1-3 mL HNO_3 and 1-3 mL HF were added into the Teflon bomb; (4) Teflon bomb was putted in a stainless steel pressure jacket and heated to 190 ℃ in an oven for >24 hours; (5) After cooling, the Teflon bomb was opened and placed on a hotplate at 140 ℃ and evaporated to incipient dryness, and then 1 mL HNO_3 was added and evaporated to dryness again; (6) The sample was dissolved in 1.0 mL of 1.0 M HBr.

Column chemistry: After centrifugation, the supernatant solution was loaded into an ion-exchange column packed with AG resin. After complete draining of the sample solution, columns were rinsed with 1.0 M HBr to remove undesirable matrix elements. Finally, the Pb fraction was eluted using 6.0 M HCl and gently evaporated to dryness prior to mass spectrometric measurement.

Pb isotope analyses were performed on a Neptune Plus MC-ICP-MS (Thermo Fisher Scientific, Dreieich, Germany). The Neptune Plus, a double focusing MC-ICP-MS, was equipped with seven fixed electron multiplier ICs and nine Faraday cups fitted with 10^{11} Ω resistors. The faraday collector configuration of the mass system was composed of an array to

monitor ^{204}(Pb+Hg), ^{206}Pb, ^{207}Pb, ^{208}Pb, ^{203}Tl, ^{205}Tl and ^{202}Hg. The large dry interface pump (120 $m^3\,hr^{-1}$ pumping speed) and newly designed X skimmer cone and Jet sample cone were used to increase the instrumental sensitivity. A Pb single element solution from Alfa (Alfa Aesar, Karlsruhe, Germany) was used to optimize instrument operating parameters. An aliquot of the international standard solution of 100 μg/L NIST 981 was regularly used for evaluating the reproducibility and accuracy of the instrument. Typically, the signal intensities of $^{208}Pb^{+}$ in NIST 981 were > ~6.0 V. The Pb isotopic data were acquired in the static mode at low resolution. The routine data acquisition consisted of ten blocks of 10 cycles (4.194 s of integration time per cycle). The total time of one measurement lasted about 7 minutes.

The exponential law, which was initially developed for TIMS measurement (Russell et al. 1978) and remains the most widely accepted and utilized with MC-ICP-MS, was used to assess the instrumental mass discrimination in this study. Mass discrimination correction was carried out via normalization to a $^{205}Tl/^{203}Tl$ ratio of 2.38714 (the certified value of NIST SRM 997). All data reduction for the MC-ICP-MS analysis of Pb isotope ratios was conducted using "Iso-Compass" software (Zhang et al. 2020). Because of the difference in mass bias behaviors between Pb and Tl, all measured $^{20x}Pb/^{204}Pb$ ratios of unknown samples were normalized to the well-accepted NIST 981 values of $^{208}Pb/^{204}Pb$=36.7262 ± 31, $^{207}Pb/^{204}Pb$=15.5000 ± 13, $^{206}Pb/^{204}Pb$=16.9416 ± 13 (2SD; Baker et al. 2004). One NIST 981 standard was measured every ten samples analyzed. Analyses of NIST 981 standard yielded external precisions of 0.03% (2RSD) for $^{20x}Pb/^{204}Pb$ ratios. In addition, the USGS reference materials BCR-2 yielded results of $^{208}Pb/^{204}Pb$=38.739 ± 14, $^{207}Pb/^{204}Pb$=15.627 ± 5, $^{206}Pb/^{204}Pb$=18.759 ± 6 (2SD), respectively, which is identical within error of 0.03% to their published values (Weis et al., 2006).

5. Analytical methods of Zn isotope

Whole-rock Zn isotope data were measured at Wuhan Shangpu Solution Analytical Technology Co., Ltd.

Sample digestion: Approximately 50 mg of sample powders were weighed into in-house PTFE-lined steel bombs and dissolved in 1mL HNO_3 and 1 mL HF in the oven at 190 ℃ for 48 hours. The digest contents were then dried and redissolved with 1 mL HNO_3. This step was repeated twice to completely remove HF. After that, 1 mL HNO_3 and 2 mL MQ-water were added, and the bombs were screwed and placed in the oven overnight at 190 ℃. The digests were dried and redissolved with 1 mL HCl to convert the sample from nitrate form to chloride form. Finally, the digests were evaporated to dryness and redissolved in 1mL 8M HCl+0.001% H_2O_2 in preparation for ion exchange separation.

Chemical purification: Zinc was purified by a single column ion-exchange chromatography using Bio-Rad strong anion resin AG-MP-1M (Zhu et al., 2019). 2 mL of pre-cleaned resin was loaded onto the cleaned column. Matrix elements were eluted in the first 10 mL 8 N HCl. Then, after the iron was eluted by 18 mL of 2 N HCl + 0.001% H_2O_2, the zinc fraction was collected in 10 mL 0.5 N HNO_3. The recovery for Zn is > 99%. The total procedural blanks are always <10 ng for Zn based on long-term analyses, which are considered negligible. The Zn fraction was evaporated to dryness, dissolved in 2% HNO_3, and then re-evaporated to dryness and redissolved in 2% HNO_3 to remove all chlorine prior to isotope analysis.

Zinc isotopic ratios were measured using the Neptune plus MC-ICP-MS. Samples were introduced at a concentration of 200 ppb in 2% HNO_3 using wet plasma method. Standard-sample bracketing (SSB) method was used in order to correct for instrumental mass fractionation. Zn isotopic data are reported in standard notation in per mil relative to standard reference material JMC- 3-0749L, respectively:

$\delta^{66}Zn = [(^{66}Zn/^{64}Zn)_{sample} / (^{66}Zn/^{64}Zn)_{JMC\ 3\text{-}0749L} -1] \times 1000$ (‰)

The long-term external reproducibility for $\delta^{66}Zn$ measurements is better than ± 0.05‰ (2SD), respectively, based on repeated analyses of natural samples and synthetic solutions. Several international rock standards were analyzed for Zn isotopes during the course of this study. The reference materials analyzed in this study yielded results (BHVO-2: $\delta^{66}Zn$ = 0.34‰ ± 0.02‰; BCR-2: $\delta^{66}Zn$ = 0.27‰ ±0.01‰) identical within errors with the literature values (Chen et al., 2016; Zhu et al., 2019). Each sample was measured three times and the average of those values is reported.

6. Analytical methods of Mg isotope

Whole-rock Mg isotope data were measured at State Key Laboratory of Continental Dynamics, Northwestern University, Xi'an, China. All of the chemical preparations were conducted on class-100 workbenches inside a class-1000 clean laboratory. Before measurement, sample digestion and chemical purification of Mg were conducted, which are mainly based on Bao et al., (2019; 2020).

Sample digestion: 0.1-15 mg of sample powders were weighed and fully digested to obtain 25 μg Mg for chemical purification based on the MgO content. The samples were dissolved in 10mL Savillex Teflon beakers with a mixture of concentrated HF-HNO_3 (3:1, v/v). The capped beakers were heated at a temperature of 120 ℃ on a hot plate in the class-100 workbenches, and the solutions were evaporated to dryness. In order to achieve 100% dissolution, the dried samples were refluxed with concentrated HNO_3 to remove residual fluorides and were then again evaporated to dryness. This dried residue was finally dissolved in 1mL of 1 mol/L HNO_3, which was transferred into 2mL centrifuge tubes for precipitation.

Chemical purification: 1 mL of a 4 mol/L sodium hydroxide solution was added to maintain a pH of 14, leading to $Mg(OH)_2$ in an ultrasonic bath for 15 min, and afterward, a coloured precipitate formed at this stage. After centrifugation for 15 min at 10000 rpm, the supernatant was discarded. The precipitation and centrifugation procedure was performed twice in order to eliminate almost all K cations. The solid precipitate was finally dissolved in 1 mL of 12 mol/L HCl and centrifuged for chromatographic chemistry. Subsequently, the dissolved rock solutions containing 25 μg of Mg were passed through two columns containing ion-exchange resins to eliminate matrix elements. Mg purification was first performed in Bio-Rad columns loaded with 2 mL of Bio-Rad 200-400 mesh AG50W-X12 cation exchange resin. The resin was conditioned with 5 mL of 12 mol/L HCl before the chemical separation procedure. The dissolved rock samples containing 25 μg of Mg were loaded into the column. After loading the sample, 5 mL of 12 mol/L HCl were loaded to collect the eluant, which contains Mg, Na, Al and other major cations. Then the collected eluant was evaporated to dryness, and the residues were dissolved in 0.5 mL of 1 mol/L HNO_3 + 0.5 mol/L HF for the second column. The second stage was carried out using Bio-Rad columns loaded with 0.5 mL of Bio-Rad 200-400 mesh AG50W-X12 cation exchange resin, which had been pre-cleaned with 5 mL of 12 mol/L HCl and Milli-Q H_2O and then conditioned with 5 mL of 1 mol/L HNO_3 + 0.5 mol/L HF. The sample after dissolution in 0.5 mL of 1 mol/L HNO_3 + 0.5 mol/L HF was loaded onto the resin. All of the Mg was then eluted with 3 mL of 6 mol/L HCl. The collected solutions were then evaporated at 80 ℃ to dryness, and the residues were dissolved in 2% HNO_3 for isotope ratio measurements. The recovery for Mg is >99% and the total procedural blanks are systematically <30 ng for Mg based on long-term analyses, which are considered negligible.

Mg isotope ratios were measured using a Nu Plasma II MC-ICPMS (Nu Instruments, Wrexham, UK). The Nu Plasma II is a double-focusing mass spectrometer with sixteen Faraday cups and five full-size discrete dynode multipliers. During the analyses, L5, Ax, and H5 Faraday cups were used to collect ^{24}Mg, ^{25}Mg and ^{26}Mg, respectively. All Mg solutions were diluted with 2% (v/v) HNO_3 at room temperature in order to achieve a Mg concentration of 0.5 μg/g in the final solution. A "wet" plasma with a wet cone and a GE 100 μL/min quartz nebuliser was utilized to measure the Mg isotopes. The signal sensitivity for ^{24}Mg was typically about 8 V/ppm in the low-resolution mode. A block of analysis consisted of 25 cycles of data with an integration time of 10 s per cycle. The standard-sample-standard bracketing method (SSB) was used to correct the instrumental mass bias during the analyses. The Mg isotopic ratios were normalized to the international DSM3 Mg purified solution with homogeneous Mg isotopes, prepared and provided by Galy et al (2003). The results were expressed as a per mil deviation of the isotopic composition of the DSM3 standard:

$$\delta^{26}Mg = [(^{26}Mg/^{24}Mg)_{sample} / (^{26}Mg/^{24}Mg)_{DSM3} - 1] \times 1000 \ (‰)$$

The reference materials analyzed in this study yielded results (BCR-2: $\delta^{26}Mg$ = -0.20‰ ± 0.06‰; JDO-1: $\delta^{26}Mg$ = -2.37‰ ± 0.04‰; Alfa Mg: $\delta^{26}Mg$ = -3.88‰ ± 0.02‰) identical within errors with the literature values (Teng, 2017; Bao et al., 2019). Each sample was measured four times and the average of those values is reported.

7. Mixing model

We used a mixing model of depleted mid-ocean-ridge basalt mantle (DMM) and recycled materials in the Figs. 3B and 3C, and Fig. S4. The mixing lines among DMM, dolomite, magnesite and siliceous sediments in the Figs. 3B and 3C, the mixing line between the samples which are least affected by interaction and carbonated peridotites in the Figs. 3B and 3C, and the

mixing lines among DMM, siliceous sediments and magnesite in Fig. S4 are calculated by the geoplot (a geospatial data visualization software), based on the AFC Model of Depaolo (Depaolo et al, 1981). Values used for mixing end-members and associated references are listed in Table. S4.

In Figs. 3B and 3C, although it is uncertain to argue the end-members and their mixing proportions, the Zn-Sr and Zn-Nd isotopic compositions of the samples with minor trans-mantle effect (interaction with the ambient mantle) provide an approximate result. About 10-15% carbonate-bearing sediments (include carbonate and silicate) are indeed calculated to account for the isotopes. Therein, the pure carbonate (magnesite) was limited in range of 6-7% (Figs. 3B and 3C). This proportion of carbonate added is reasonable, like the previous study (5-10%; He at al., 2019). The mixing curves between DMM and dolomite are used for comparison.

Supplementary Figures

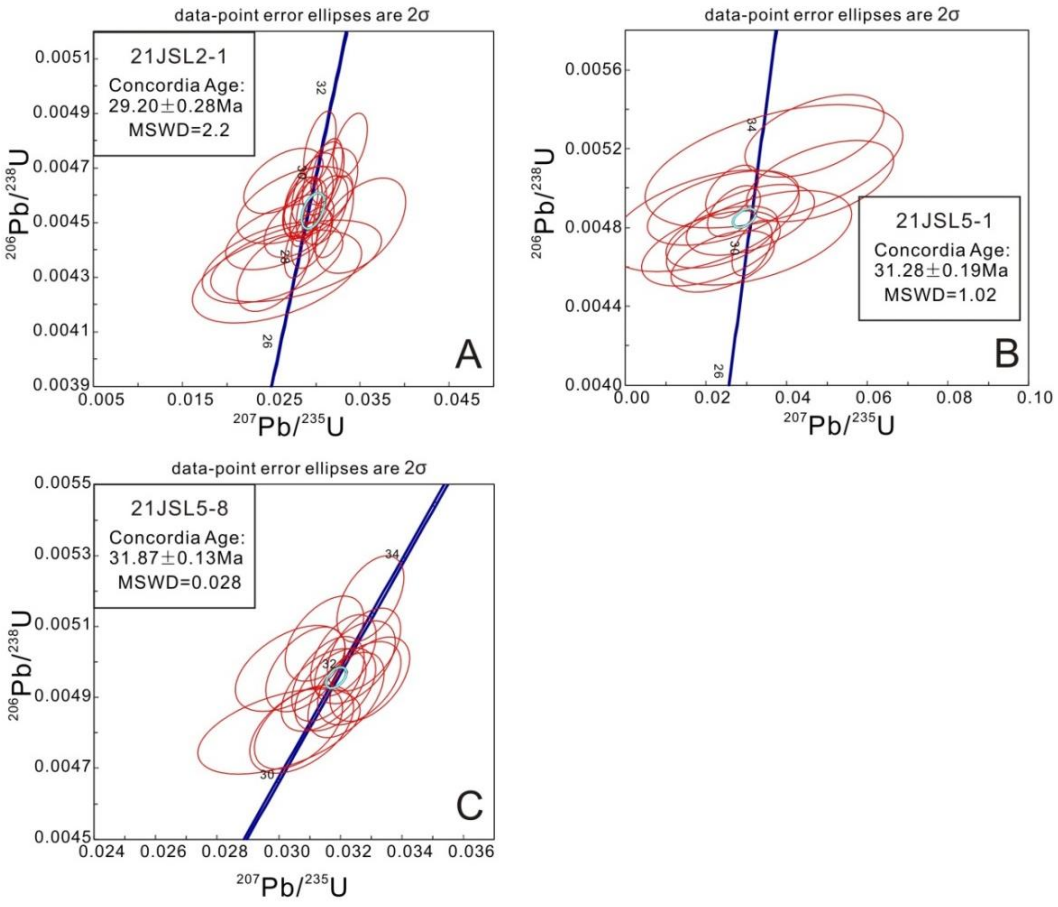

Fig. S1. Zircon U-Pb Concordia diagrams and relative probability for the samples.

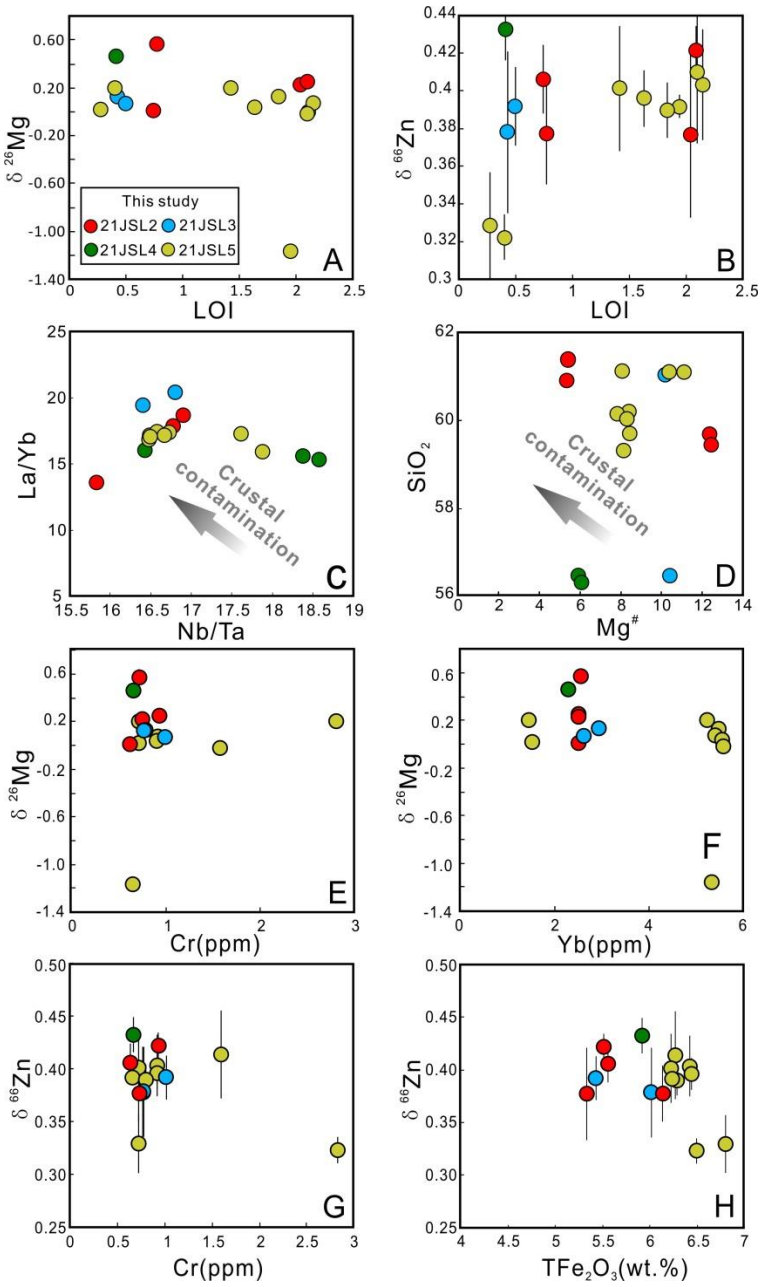

Fig. S2. (A, B) Plots of loss-on-ignition (LOI) versus $\delta^{26}Mg$ and $\delta^{66}Zn$ of samples. (C) Plots of La/Yb versus Nb/Ta of samples. (D) Plots of SiO_2 versus $Mg^{\#}$ of samples. (E, F) Plots of $\delta^{26}Mg$ versus Cr and Yb of samples. Fractional crystallization of spinel and garnet did not significantly influence Mg isotopic compositions of samples. (G, H) Plots of $\delta^{66}Zn$ versus Cr and TFe_2O_3 of samples. Fractional crystallization of spinel and Fe-Ti oxides did not significantly influence Zn isotopic compositions of samples.

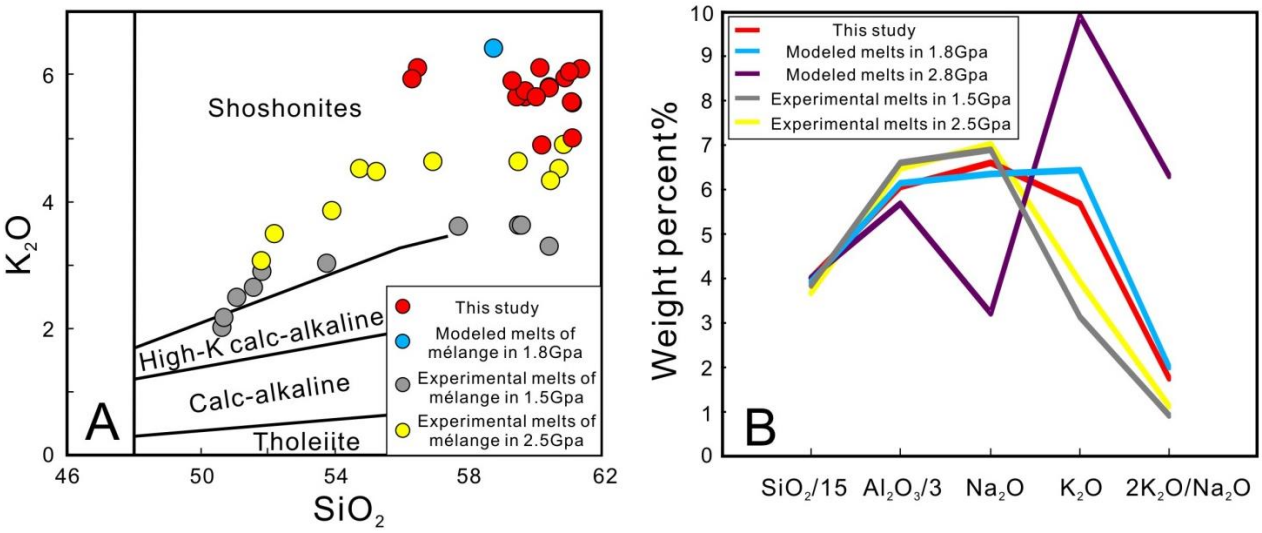

Fig. S3. (A) Plots of K_2O versus SiO_2. The data for modeled melts of mélange are from Wang et al. (2022). The data for experimental melts for mélange are from Cruz-Uribe et al. (2018). (B) Compositions of major-element oxides. K_2O contents of modeled and experimental melts increases as pressure increases (Wang et al., 2022). K_2O contents of samples are higher than experimental melts, reflect a relatively high pressure environment.

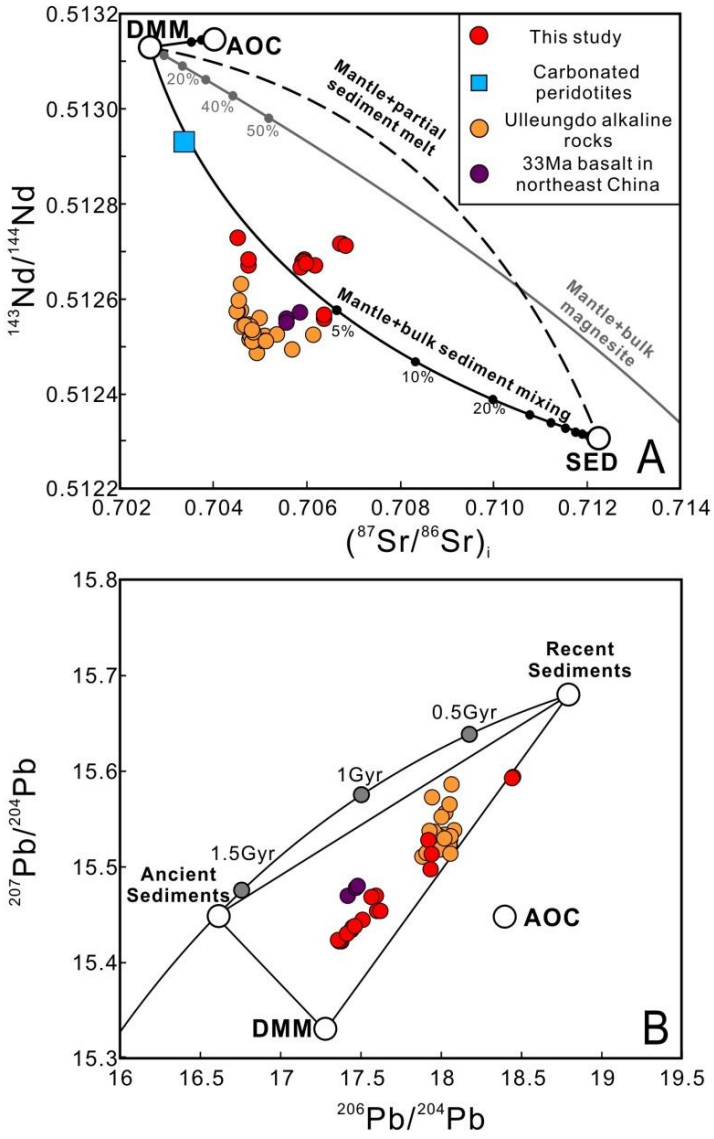

Fig. S4. (A) Plots of $(^{87}Sr/^{86}Sr)_i$ versus $^{143}Nd/^{144}Nd$. Solid curve represents mixing line between DMM and bulk sediment, while dotted curve represents mixing trajectories between DMM and sediment melt. Values of mixing end members and associated references are listed in Table S4 (see footnote 1). Both samples and the Ulleungdo alkaline rocks plot in the DMM-bulk sediments mixing line and far away from the DMM–sediment melt mixing trajectories, which is consistent with the geochemical characteristic of mélange melting (Nielsen and Marschall, 2017). Mélange in this study expectedly have experienced the mélange-mantle interaction in the

asthenosphere (≥4.5Gpa), so it can be inferred that the carbonate type of mélange is mainly magnesite (Dalton et al., 1993). In Fig. 3B, magnesite is also necessary to account for the isotopic compositions of mélange. Sr and Nd contents of magnesite are relatively low compared to the mantle (Table. S4), so addition of magnesite is hard to significantly affect the Sr-Nd isotopic compositions of the mantle. (B) Plots of $^{206}Pb/^{204}Pb$ versus $^{207}Pb/^{204}Pb$ (modified from Kuritani et al., 2013). Data for 33Ma basalts in northeast China are from Dong et al. (2023). Gray solid circles represent sediments with different age, which are from Kuritani et al. (2013).

Table S1: Zircon SIMS U-Pb data for the Oligocene alkaline intermediate igneous rocks within the northeast China.

Spot analysis	Th	U	Th/U	$^{207}Pb/^{206}Pb$		$^{207}Pb/^{235}U$		$^{206}Pb/^{238}U$		$^{207}Pb/^{206}Pb$		$^{207}Pb/^{235}U$		$^{206}Pb/^{238}U$	
	ppm	ppm		Ratio	1σ	Ratio	1σ	Ratio	1σ	Ma	1σ	Ma	1σ	Ma	1σ
21JSL2-1-1	3470	1916	1.81	0.04828	0.00163	0.03122	0.00118	0.00469	0.00008	113	78	31	1	30	1
21JSL2-1-2	540	671	0.80	0.04389	0.00679	0.02762	0.00431	0.00456	0.00009	-117	343	28	4	29	1
21JSL2-1-3	1541	1469	1.05	0.04220	0.00646	0.02589	0.00399	0.00445	0.00008	-215	346	26	4	29	1
21JSL2-1-4	282	413	0.68	0.04185	0.00865	0.02512	0.00522	0.00435	0.00010	-236	454	25	5	28	1
21JSL2-1-5	790	931	0.85	0.04949	0.00254	0.03102	0.00169	0.00455	0.00008	171	116	31	2	29	1
21JSL2-1-6	508	1449	0.35	0.05134	0.00175	0.03386	0.00128	0.00478	0.00008	256	76	34	1	31	0
21JSL2-1-7	3425	1981	1.73	0.04814	0.00231	0.02950	0.00150	0.00444	0.00007	106	110	30	1	29	0
21JSL2-1-8	354	319	1.11	0.05661	0.00521	0.03504	0.00335	0.00449	0.00012	476	192	35	3	29	1
21JSL2-1-9	2037	1584	1.29	0.04623	0.00162	0.03044	0.00120	0.00478	0.00009	0	92	30	1	31	1
21JSL2-1-10	694	752	0.92	0.05115	0.00220	0.03189	0.00154	0.00452	0.00010	248	96	32	2	29	1
21JSL2-1-11	1243	1434	0.87	0.04539	0.00412	0.02810	0.00260	0.00449	0.00008	-35	207	28	3	29	0
21JSL2-1-12	420	661	0.63	0.04613	0.00283	0.02910	0.00187	0.00457	0.00009	0	146	29	2	29	1
21JSL2-1-13	4078	2107	1.94	0.04106	0.00454	0.02634	0.00295	0.00465	0.00008	-284	261	26	3	30	1
21JSL2-1-14	426	619	0.69	0.04804	0.00416	0.03056	0.00274	0.00461	0.00011	101	193	31	3	30	1
21JSL2-1-15	647	365	1.77	0.04320	0.01053	0.02563	0.00628	0.00430	0.00011	-156	516	26	6	28	1
21JSL2-1-17	3019	1816	1.66	0.04795	0.00223	0.03083	0.00155	0.00466	0.00009	97	107	31	2	30	1
21JSL2-1-18	2548	1997	1.28	0.04504	0.00191	0.02830	0.00128	0.00456	0.00007	-53	100	28	1	29	0
21JSL2-1-21	730	1096	0.67	0.04651	0.00184	0.02831	0.00122	0.00441	0.00008	24	92	28	1	28	0
21JSL2-1-22	3595	2103	1.71	0.04647	0.00203	0.02913	0.00136	0.00455	0.00007	22	102	29	1	29	0
21JSL2-1-23	1061	1796	0.59	0.04612	0.00173	0.02888	0.00121	0.00454	0.00008	0	92	29	1	29	1
21JSL2-1-24	562	859	0.65	0.04233	0.00443	0.02518	0.00269	0.00431	0.00009	-207	244	25	3	28	1
21JSL2-1-25	2497	2137	1.17	0.04659	0.00133	0.02925	0.00096	0.00455	0.00007	28	67	29	1	29	0

Table S1 *(Continued)*

Spot analysis	Th	U	Th/U	$^{207}Pb/^{206}Pb$		$^{207}Pb/^{235}U$		$^{206}Pb/^{238}U$		$^{207}Pb/^{206}Pb$		$^{207}Pb/^{235}U$		$^{206}Pb/^{238}U$	
	ppm	ppm		Ratio	1σ	Ratio	1σ	Ratio	1σ	Ma	1σ	Ma	1σ	Ma	1σ
21JSL2-1-26	398	665	4.68	0.04682	0.00250	0.02984	0.00169	0.00462	0.00009	40	123	30	2	30	1
21JSL2-1-27	396	557	7.25	0.04620	0.01051	0.02777	0.00635	0.00436	0.00010	0	480	28	6	28	1
21JSL5-1-01	5780	1235	18.73	0.17398	0.00368	0.03096	0.01049	0.00484	0.00012	0	677	31	10	31	1
21JSL5-1-03	3698	510	7.87	0.13774	0.00491	0.04683	0.01137	0.00527	0.00014	758	441	46	11	34	1
21JSL5-1-06	8114	433	0.40	0.11601	0.00477	0.01950	0.01557	0.00483	0.00017	-1237	1548	20	16	31	1
21JSL5-1-07	4996	635	4.44	0.14210	0.00445	0.02117	0.01134	0.00469	0.00013	-900	1106	21	11	30	1
21JSL5-1-10	30	74	0.70	0.06136	0.00320	0.28646	0.02491	0.03749	0.00062	429	180	256	20	237	4
21JSL5-1-11	15591	3509	4.48	0.08006	0.00199	0.02687	0.00433	0.00488	0.00009	-357	357	27	4	31	1
21JSL5-1-12	118	168	0.43	0.05212	0.00351	0.13762	0.01327	0.02109	0.00035	66	212	131	12	135	2
21JSL5-1-13	4421	988	3.65	0.19993	0.00415	0.02418	0.01238	0.00490	0.00012	-646	1022	24	12	32	1
21JSL5-1-14	268	627	11.24	0.05604	0.00280	0.03136	0.00328	0.00470	0.00009	121	226	31	3	30	1
21JSL5-1-16	7966	2182	5.16	0.08653	0.00191	0.02641	0.00433	0.00498	0.00009	-454	383	26	4	32	1
21JSL5-1-17	5670	504	12.03	0.17493	0.00543	0.04823	0.01204	0.00504	0.00014	912	441	48	12	32	1
21JSL5-1-18	6773	1313	14.96	0.14516	0.00456	0.02389	0.00915	0.00475	0.00010	-596	810	24	9	31	1
21JSL5-1-19	4389	365	6.39	0.17100	0.00636	0.03311	0.01516	0.00475	0.00016	221	811	33	15	31	1
21JSL5-1-21	4447	297	4.68	0.19644	0.00805	0.03680	0.02109	0.00511	0.00021	295	952	37	21	33	1
21JSL5-1-22	6649	1041	7.25	0.14510	0.00389	0.02408	0.00844	0.00482	0.00008	-504	742	24	8	30	1
21JSL5-8-01	1519	1361	1.12	0.05214	0.00173	0.03301	0.00139	0.00467	0.00008	250	86	33	1	30	1
21JSL5-8-02	974	1103	0.88	0.04956	0.00295	0.03120	0.00241	0.00488	0.00009	0	189	31	2	31	1
21JSL5-8-03	2157	1815	1.19	0.05052	0.00212	0.03079	0.00154	0.00455	0.00007	150	107	31	2	29	0
21JSL5-8-04	1350	1210	1.12	0.05831	0.00193	0.02650	0.00298	0.00459	0.00008	-235	259	27	3	30	1
21JSL5-8-05	244	594	0.41	0.04962	0.00255	0.03107	0.00222	0.00473	0.00009	79	155	31	2	30	1
21JSL5-8-06	147	260	0.56	0.05663	0.00408	0.01912	0.00840	0.00482	0.00014	-1291	1026	19	8	31	1

Table S1 *(Continued)*

Spot analysis	Th	U	Th/U	$^{207}Pb/^{206}Pb$		$^{207}Pb/^{235}U$		$^{206}Pb/^{238}U$		$^{207}Pb/^{206}Pb$		$^{207}Pb/^{235}U$		$^{206}Pb/^{238}U$	
	ppm	ppm		Ratio	1σ	Ratio	1σ	Ratio	1σ	Ma	1σ	Ma	1σ	Ma	1σ
21JSL5-8-07	1976	1945	1.02	0.04837	0.00140	0.03102	0.00103	0.00465	0.00008	117	67	31	1	30	0
21JSL5-8-08	503	714	0.70	0.05181	0.00243	0.02798	0.00315	0.00473	0.00012	-173	254	28	3	30	1
21JSL5-8-09	925	1234	0.75	0.04831	0.00185	0.03231	0.00136	0.00485	0.00008	114	88	32	1	31	1
21JSL5-8-10	4449	3161	1.41	0.04947	0.00110	0.03176	0.00104	0.00481	0.00008	95	65	32	1	31	1
21JSL5-8-11	184	444	0.41	0.05119	0.00311	0.03322	0.00217	0.00471	0.00011	249	134	33	2	30	1
21JSL5-8-12	1305	1639	0.80	0.05156	0.00165	0.03164	0.00152	0.00468	0.00008	151	102	32	2	30	1
21JSL5-8-13	355	560	0.63	0.05795	0.00329	0.03138	0.00377	0.00463	0.00011	156	255	31	4	30	1
21JSL5-8-14	2218	1779	1.25	0.04878	0.00147	0.03141	0.00110	0.00467	0.00009	137	69	31	1	30	1
21JSL5-8-15	759	652	1.16	0.05315	0.00277	0.02681	0.00428	0.00467	0.00010	-246	359	27	4	30	1
21JSL5-8-16	2570	2024	1.27	0.04688	0.00160	0.03116	0.00118	0.00482	0.00008	43	80	31	1	31	1
21JSL5-8-17	806	1318	0.61	0.04811	0.00202	0.03135	0.00141	0.00473	0.00008	105	97	31	1	30	0
21JSL5-8-18	595	816	0.73	0.05552	0.00230	0.03262	0.00225	0.00469	0.00009	214	147	33	2	30	1
21JSL5-8-19	304	591	0.51	0.05473	0.00301	0.03235	0.00269	0.00462	0.00009	234	176	32	3	30	1
21JSL5-8-20	326	732	0.44	0.05252	0.00240	0.02690	0.00333	0.00465	0.00009	-228	283	27	3	30	1
21JSL5-8-21	1989	1681	1.18	0.05080	0.00154	0.03073	0.00149	0.00465	0.00007	94	105	31	1	30	0
21JSL5-8-22	1492	1297	1.15	0.04900	0.00171	0.03097	0.00149	0.00475	0.00008	62	103	31	1	31	1
21JSL5-8-23	1290	1339	0.96	0.05031	0.00179	0.03051	0.00181	0.00476	0.00008	23	130	31	2	31	1
21JSL5-8-24	1645	1982	0.83	0.04703	0.00136	0.03105	0.00102	0.00479	0.00008	51	67	31	1	31	0
21JSL5-8-25	452	837	0.54	0.04774	0.00212	0.03142	0.00160	0.00477	0.00012	87	102	31	2	31	1
21JSL5-8-26	338	662	0.51	0.05378	0.00255	-	-	0.00469	0.00009	-	-	-	-	30	1
21JSL5-8-27	459	692	0.66	0.05282	0.00254	0.03318	0.00213	0.00471	0.00010	243	134	33	2	30	1
21JSL5-8-28	684	1046	0.65	0.05295	0.00233	0.03412	0.00183	0.00478	0.00009	276	112	34	2	31	1

Table S2: Major (wt. %) and trace elements (ppm) and Sr-Nd-Pb isotope data for the Oligocene alkaline intermediate igneous rocks within the northeast China.

Sample	21JSL2-1	21JSL2-2	21JSL2-4	21JSL2-5	21JSL3-1
Lithology	syenite	syenite	syenite	syenite	syenite
SiO_2	61.38	60.90	59.69	59.45	60.43
TiO_2	0.48	0.53	0.50	0.48	0.40
Al_2O_3	17.73	17.58	18.12	18.08	18.25
TFe_2O_3	5.52	6.08	5.42	5.22	5.40
MnO	0.12	0.13	0.14	0.14	0.15
MgO	0.16	0.17	0.38	0.37	0.31
CaO	1.47	1.65	2.53	2.55	1.87
Na_2O	6.28	6.24	5.87	5.95	6.75
K_2O	6.05	5.91	5.56	5.53	5.77
P_2O_5	0.04	0.04	0.14	0.14	0.12
LOI	0.74	0.77	2.09	2.04	0.50
SUM	99.96	99.99	100.44	99.92	99.93
Li	10.62	12.11	14.65	13.30	6.89
Be	3.05	3.33	3.45	3.55	4.06
Sc	1.92	2.02	3.27	2.99	2.15
V	2.37	2.64	1.33	1.61	2.58
Cr	0.63	0.71	0.93	0.76	1.01
Co	0.75	0.83	1.60	1.60	1.41
Ni	0.47	0.44	0.47	0.33	1.28
Cu	2.10	2.19	4.06	3.82	3.86
Zn	78.27	84.82	95.08	92.81	93.73
Ga	30.37	29.93	29.05	28.85	28.67
Rb	77.75	76.95	70.25	67.68	70.26
Sr	28.76	28.46	414.81	438.09	270.21
Y	24.59	24.60	27.48	26.73	29.50
Zr	336.96	325.26	381.80	376.70	431.82
Nb	73.85	74.50	65.49	63.76	76.90
Sn	3.03	3.15	2.85	3.19	3.29
Cs	0.49	0.59	0.55	0.50	0.49
Ba	36.31	37.60	676.40	670.23	331.75
La	34.10	34.73	46.55	44.73	53.51
Ce	64.93	68.39	91.37	87.08	104.46
Pr	7.33	7.72	10.33	9.94	11.74
Nd	26.02	27.74	38.20	36.26	42.56
Sm	5.44	5.62	8.00	7.62	8.51
Eu	0.68	0.61	2.76	2.77	1.99
Gd	4.49	4.61	6.42	6.20	6.84
Tb	0.75	0.76	0.98	0.97	1.05

Table S2 *(Continued)*

Sample	21JSL2-1	21JSL2-2	21JSL2-4	21JSL2-5	21JSL3-1
Lithology	**syenite**	**syenite**	**syenite**	**syenite**	**syenite**
Dy	4.54	0.85	2.49	0.36	2.51
Ho	4.47	0.87	2.45	0.38	2.55
Er	5.57	1.03	2.69	0.38	2.49
Tm	5.31	0.99	2.64	0.38	2.50
Yb	5.92	1.08	2.92	0.40	2.62
Lu	4.54	0.85	2.49	0.36	2.51
Hf	4.47	0.87	2.45	0.38	2.55
Ta	5.57	1.03	2.69	0.38	2.49
Tl	5.31	0.99	2.64	0.38	2.50
Pb	5.92	1.08	2.92	0.40	2.62
Th	4.54	0.85	2.49	0.36	2.51
U	4.47	0.87	2.45	0.38	2.55
$^{87}Rb/^{86}Sr$	2.703	2.704	0.169	0.154	0.260
$^{87}Sr/^{86}Sr$	0.707969	0.707921	0.704792	0.704787	0.704623
±2σ	0.000006	0.000007	0.000006	0.000007	0.000006
$(^{87}Sr/^{86}Sr)_i$	0.706752	0.706704	0.704716	0.704717	0.704506
$^{147}Sm/^{144}Nd$	0.126	0.123	0.127	0.127	0.121
$^{143}Nd/^{144}Nd$	0.512718	0.512719	0.512673	0.512683	0.512729
±2σ	0.000005	0.000005	0.000007	0.000005	0.000006
εNd(0)	1.56	1.58	0.68	0.88	1.78
εNd(t)	1.85	1.88	0.97	1.16	2.08
T_{1DM}(Ma)	754	721	835	821	692
T_{2DM}(Ma)	691	689	763	647	672
$f_{Sm/Nd}$	-0.36	-0.38	-0.36	-0.35	-0.39
$^{206}Pb/^{204}Pb$	17.3850	17.3644	17.5983	17.5673	17.6013
$^{207}Pb/^{204}Pb$	15.4232	15.4229	15.4710	15.4693	15.4544
$^{208}Pb/^{204}Pb$	38.1016	38.0983	38.1377	38.1326	38.3779
$(^{206}Pb/^{204}Pb)_i$	17.385	17.3644	17.5983	17.5673	17.6013
$(^{207}Pb/^{204}Pb)_i$	15.4232	15.4229	15.471	15.4693	15.4544
$(^{208}Pb/^{204}Pb)_i$	38.1016	38.0983	38.1377	38.1326	38.3779

Table S2 *(Continued)*

Sample	21JSL3-2	21JSL4-5	21JSL4-6	21JSL4-7	21JSL5-1
Lithology	**syenite**	**syenite**	**nepheline syenite**	**nepheline syenite**	**syenite**
SiO_2	60.42	61.04	56.48	56.32	61.12
TiO_2	0.45	0.55	0.13	0.14	0.39
Al_2O_3	17.93	18.09	21.56	21.39	17.88
TFe_2O_3	6.01	5.92	4.58	4.98	6.15
MnO	0.17	0.12	0.11	0.11	0.13
MgO	0.35	0.18	0.14	0.16	0.27
CaO	2.05	1.66	1.05	1.19	0.93
Na_2O	6.64	6.33	9.13	8.87	6.99
K_2O	5.78	6.04	6.06	5.88	4.96
P_2O_5	0.14	0.05	0.05	0.05	0.12
LOI	0.43	0.41	0.99	1.19	1.42
SUM	100.38	100.39	100.29	100.27	100.34
Li	8.50	15.86	10.49	26.32	13.91
Be	4.42	4.62	4.92	5.28	5.31
Sc	2.39	2.44	1.12	1.17	2.74
V	2.53	4.35	0.69	0.99	2.34
Cr	0.77	0.66	3.61	0.84	0.72
Co	1.57	0.88	0.71	0.70	1.66
Ni	0.40	0.49	0.36	0.33	0.40
Cu	4.02	2.81	1.98	1.82	4.91
Zn	106.29	75.38	87.94	93.31	138.11
Ga	28.57	29.90	41.51	42.42	35.70
Rb	70.02	69.76	131.37	127.73	92.54
Sr	265.91	25.95	6.59	8.57	98.25
Y	33.38	23.30	25.87	26.63	55.71
Zr	513.34	326.30	452.63	446.98	960.23
Nb	85.84	65.10	60.67	63.11	141.19
Sn	3.79	3.87	4.47	4.68	7.75
Cs	0.49	0.99	0.69	0.85	0.34
Ba	325.98	66.10	4.64	4.83	236.83
La	57.26	36.50	47.72	47.24	91.21
Ce	112.14	70.12	96.40	96.99	177.24
Pr	12.48	7.83	10.76	10.85	19.66
Nd	45.03	28.27	37.36	38.25	66.39
Sm	9.06	5.64	7.22	7.56	13.59
Eu	2.10	0.83	0.31	0.33	1.36
Gd	7.27	4.76	5.73	5.78	11.07
Tb	1.16	0.78	0.90	0.97	1.80

Table S2 *(Continued)*

Sample	21JSL3-2	21JSL4-5	21JSL4-6	21JSL4-7	21JSL5-1
Lithology	**syenite**	**syenite**	**nepheline syenite**	**nepheline syenite**	**syenite**
Dy	6.55	4.40	5.21	5.39	10.68
Ho	1.22	0.84	0.95	0.99	2.10
Er	3.25	2.28	2.66	2.76	5.53
Tm	0.46	0.35	0.42	0.42	0.81
Yb	2.95	2.27	3.06	3.08	5.24
Lu	0.42	0.35	0.49	0.51	0.74
Hf	10.76	7.83	10.76	10.54	20.90
Ta	5.23	3.96	3.30	3.40	8.44
Tl	0.23	0.22	0.39	0.40	0.39
Pb	8.33	9.05	6.23	6.56	13.22
Th	8.43	5.39	6.11	7.70	15.64
U	2.44	1.50	1.57	1.89	3.90
$^{87}Rb/^{86}Sr$	0.263	2.688	-	-	0.942
$^{87}Sr/^{86}Sr$	0.704600	0.708022	-	-	0.706356
±2σ	0.000006	0.000008	-	-	0.000005
$(^{87}Sr/^{86}Sr)_i$	0.704481	0.706812	-	-	0.705932
$^{147}Sm/^{144}Nd$	0.122	0.121	-	-	0.124
$^{143}Nd/^{144}Nd$	0.512730	0.512712	-	-	0.512684
±2σ	0.000006	0.000006	-	-	0.000005
εNd(0)	1.79	1.44	-	-	0.90
εNd(t)	2.10	1.75	-	-	1.19
T_{1DM}(Ma)	696	718	-	-	790
T_{2DM}(Ma)	671	699	-	-	745
$f_{Sm/Nd}$	-0.382	-0.387	-	-	-0.371
$^{206}Pb/^{204}Pb$	17.6225	17.3590	-	-	17.5128
$^{207}Pb/^{204}Pb$	15.4549	15.4239	-	-	15.4461
$^{208}Pb/^{204}Pb$	38.3879	38.0947	-	-	38.3189
$(^{206}Pb/^{204}Pb)_i$	17.6225	17.3590	-	-	17.5128
$(^{207}Pb/^{204}Pb)_i$	15.4549	15.4239	-	-	15.4461
$(^{208}Pb/^{204}Pb)_i$	38.3879	38.0947	-	-	38.3189

Table S2 *(Continued)*

Sample	21JSL5-3	21JSL5-4	21JSL5-5	21JSL5-6	21JSL5-7
Lithology	**syenite**	**syenite**	**syenite**	**syenite**	**syenite**
SiO_2	59.70	60.15	60.20	59.31	60.03
TiO_2	0.38	0.39	0.37	0.37	0.37
Al_2O_3	17.81	18.02	17.77	17.92	17.74
TFe_2O_3	6.14	6.34	6.13	6.28	6.17
MnO	0.17	0.13	0.14	0.12	0.14
MgO	0.28	0.27	0.28	0.28	0.28
CaO	1.46	1.02	1.53	1.70	1.31
Na_2O	6.29	6.01	6.94	5.97	6.39
K_2O	5.62	6.01	4.81	5.77	5.54
P_2O_5	0.11	0.11	0.11	0.11	0.11
LOI	2.10	1.63	1.94	2.15	1.84
SUM	100.06	100.08	100.22	99.96	99.92
Li	17.15	20.67	15.52	20.66	18.06
Be	6.16	7.61	5.09	7.71	6.26
Sc	2.65	2.58	2.65	2.57	2.56
V	2.27	2.03	2.18	2.26	2.10
Cr	1.59	0.91	0.66	0.92	0.79
Co	1.67	1.70	1.61	1.55	1.60
Ni	0.43	0.34	0.37	0.35	0.31
Cu	4.04	4.65	3.65	5.12	3.64
Zn	141.82	148.06	139.31	142.59	143.39
Ga	36.55	36.81	36.17	37.46	36.76
Rb	101.10	107.77	84.69	101.48	100.48
Sr	101.15	102.10	98.68	161.90	94.19
Y	57.81	57.89	55.08	56.50	56.66
Zr	1000.93	1004.14	978.24	960.02	993.64
Nb	145.34	147.25	144.30	143.42	144.77
Sn	7.93	8.42	7.07	7.75	8.04
Cs	0.29	0.27	0.32	0.33	0.34
Ba	186.42	174.78	177.57	215.99	167.36
La	95.93	93.61	92.80	92.60	93.29
Ce	183.99	182.74	178.88	180.00	181.01
Pr	20.19	20.28	19.77	19.80	20.06
Nd	69.61	68.54	66.87	66.61	68.99
Sm	13.82	14.21	13.82	13.55	14.05
Eu	1.30	1.26	1.30	1.35	1.30
Gd	11.46	11.48	11.21	11.12	11.24
Tb	1.96	1.92	1.84	1.82	1.90

Table S2 *(Continued)*

Sample	**21JSL5-3**	**21JSL5-4**	**21JSL5-5**	**21JSL5-6**	**21JSL5-7**
Lithology	**syenite**	**syenite**	**syenite**	**syenite**	**syenite**
Dy	11.35	11.38	10.89	11.02	11.43
Ho	2.11	2.21	2.03	2.08	2.11
Er	5.83	5.99	5.69	5.62	5.79
Tm	0.85	0.88	0.83	0.83	0.85
Yb	5.58	5.56	5.32	5.40	5.47
Lu	0.76	0.77	0.73	0.73	0.74
Hf	21.64	21.94	21.41	21.07	21.97
Ta	8.81	8.93	8.71	8.60	8.78
Tl	0.45	0.40	0.39	0.37	0.42
Pb	14.56	15.44	16.14	15.55	14.15
Th	16.15	16.33	15.92	15.78	15.94
U	4.01	4.48	3.92	3.85	3.98
$^{87}Rb/^{86}Sr$	1.000	1.056	0.858	0.627	1.067
$^{87}Sr/^{86}Sr$	0.706345	0.706415	0.706253	0.706444	0.706469
±2σ	0.000006	0.000005	0.000005	0.000007	0.000007
$(^{87}Sr/^{86}Sr)_i$	0.705895	0.75940	0.705867	0.706162	0.705989
$^{147}Sm/^{144}Nd$	0.120	0.125	0.125	0.123	0.123
$^{143}Nd/^{144}Nd$	0.512680	0.512681	0.512668	0.512673	0.512675
±2σ	0.000006	0.000006	0.000006	0.000006	0.000006
εNd(0)	0.82	0.84	0.59	0.68	0.72
εNd(t)	1.13	1.13	0.88	0.98	1.02
T_{1DM}(Ma)	765	810	828	802	800
T_{2DM}(Ma)	750	750	770	762	759
$f_{Sm/Nd}$	-0.39	-0.36	-0.37	-0.38	-0.37
$^{206}Pb/^{204}Pb$	17.4416	17.4303	17.4516	17.4162	17.4653
$^{207}Pb/^{204}Pb$	15.4345	15.4332	15.4380	15.4314	15.4391
$^{208}Pb/^{204}Pb$	38.3024	38.2991	38.2931	38.2906	38.3085
$(^{206}Pb/^{204}Pb)_i$	17.4416	17.4303	17.4516	17.4162	17.4653
$(^{207}Pb/^{204}Pb)_i$	15.4345	15.4332	15.438	15.4314	15.4391
$(^{208}Pb/^{204}Pb)_i$	38.3024	38.2991	38.2931	38.2906	38.3085

Table S2 *(Continued)*

Sample	**21JSL5-8**	**21JSL5-9**
Lithology	**syenite**	**syenite**
SiO_2	61.10	61.10
TiO_2	0.62	0.61
Al_2O_3	16.90	16.83
TFe_2O_3	6.80	6.46
MnO	0.17	0.17
MgO	0.39	0.40
CaO	2.37	2.41
Na_2O	5.86	5.85
K_2O	5.56	5.54
P_2O_5	0.19	0.16
LOI	0.27	0.40
SUM	100.21	99.94
Li	4.18	4.40
Be	1.27	1.14
Sc	5.07	4.92
V	2.00	2.14
Cr	0.72	2.82
Co	2.19	2.07
Ni	0.33	0.46
Cu	5.46	5.20
Zn	80.37	75.79
Ga	24.75	24.99
Rb	43.12	43.13
Sr	232.13	236.23
Y	16.13	15.09
Zr	140.66	132.14
Nb	28.76	27.18
Sn	1.01	1.01
Cs	0.40	0.43
Ba	548.75	551.61
La	26.17	23.12
Ce	54.00	47.80
Pr	6.56	5.91
Nd	26.06	23.62
Sm	5.47	5.06
Eu	2.57	2.61
Gd	4.39	4.08
Tb	0.65	0.61

Table S2 *(Continued)*

Sample	21JSL5-8	21JSL5-9
Lithology	**syenite**	**syenite**
Dy	3.47	3.24
Ho	0.60	0.61
Er	1.65	1.52
Tm	0.22	0.22
Yb	1.51	1.45
Lu	0.24	0.22
Hf	3.28	3.04
Ta	1.63	1.52
Tl	0.15	0.16
Pb	3.94	3.69
Th	2.38	2.15
U	0.72	0.63
$^{87}Rb/^{86}Sr$	0.186	0.183
$^{87}Sr/^{86}Sr$	0.706461	0.706453
±2σ	0.000007	0.000007
$(\ ^{87}Sr/^{86}Sr\ )_i$	0.706377	0.706371
$^{147}Sm/^{144}Nd$	0.127	0.130
$^{143}Nd/^{144}Nd$	0.512557	0.512566
±2σ	0.000010	0.000010
εNd(0)	-1.58	-1.14
εNd(t)	-1.30	-1.13
T_{1DM}(Ma)	1040	1057
T_{2DM}(Ma)	947	934
$f_{Sm/Nd}$	-0.36	-0.34
$^{206}Pb/^{204}Pb$	18.4549	18.4466
$^{207}Pb/^{204}Pb$	15.5947	15.5929
$^{208}Pb/^{204}Pb$	38.4172	38.4118
$(^{206}Pb/^{204}Pb)_i$	18.4549	18.4466
$(^{207}Pb/^{204}Pb)_i$	15.5947	15.5929
$(^{208}Pb/^{204}Pb)_i$	38.4172	38.4118

Table S3: Mg-Zn isotope data for the Oligocene alkaline intermediate igneous rocks within the northeast China.

Sample	$\delta^{66}Zn$	±2σ	$\delta^{67}Zn$	±2σ	$\delta^{68}Zn$	±2σ
21JSL2-1	0.406	0.018	0.628	0.015	0.783	0.034
21JSL2-2	0.377	0.027	0.549	0.076	0.739	0.020
21JSL2-4	0.422	0.013	0.648	0.101	0.792	0.060
21JSL2-5	0.377	0.044	0.550	0.024	0.712	0.024
21JSL3-1	0.392	0.021	0.557	0.053	0.753	0.066
21JSL3-2	0.378	0.042	0.553	0.059	0.737	0.060
21JSL4-5	0.433	0.017	0.642	0.065	0.858	0.028
21JSL5-1	0.401	0.033	0.575	0.063	0.799	0.102
21JSL5-3	0.414	0.042	0.612	0.071	0.817	0.061
21JSL5-4	0.396	0.015	0.554	0.044	0.771	0.022
21JSL5-5	0.392	0.006	0.593	0.058	0.788	0.029
21JSL5-6	0.403	0.029	0.597	0.028	0.808	0.052
21JSL5-7	0.390	0.015	0.577	0.043	0.784	0.014
21JSL5-8	0.329	0.028	0.490	0.047	0.635	0.032
21JSL5-9	0.323	0.012	0.499	0.037	0.664	0.042

Table S3 *(Continued)*

Sample	$\delta^{25}Mg$	±2σ	$\delta^{26}Mg$	±2σ
21JSL2-1	0.01	0.03	0.01	0.03
21JSL2-2	0.31	0.04	0.57	0.06
21JSL2-4	0.14	0.01	0.25	0.05
21JSL2-5	0.12	0.04	0.23	0.04
21JSL3-1	0.04	0.02	0.07	0.06
21JSL3-2	0.05	0.04	0.13	0.05
21JSL4-5	0.24	0.03	0.47	0.04
21JSL5-1	0.11	0.02	0.21	0.03
21JSL5-3	0.00	0.06	-0.02	0.06
21JSL5-4	0.01	0.02	0.04	0.04
21JSL5-5	-0.60	0.03	-1.16	0.04
21JSL5-6	0.02	0.03	0.08	0.05
21JSL5-7	0.06	0.04	0.13	0.04
21JSL5-8	0.01	0.02	0.02	0.05
21JSL5-9	0.10	0.03	0.20	0.05

Table S4: Values and associated references for the mixing end-members in Figs. 2-3.

Name	$\delta^{66}Zn$	[Zn] (μg/g)	$\delta^{26}Mg$	$^{87}Sr/^{86}Sr$	[Sr] (μg/g)	εNd	[Nd] (μg/g)
DMM[1]	0.18	55	-	0.7025	7.7	9.8	0.58
Normal mantle[2]	0.28	-	-0.25	-	-	-	-
Silicate[3]	0.28	91	-	0.71055	121.8	-4.3	18.98
Magnesite[4]	0.91	0.28	-	0.7164	1.8	-9.7	0.1
Dolomite[5]	0.91	134	-	0.7099	1311	-	-
Carbonated peridotites[6] (average)	0.45	153	-0.33	0.70335	1111.6	5.8	62.17

[1]Zn isotope data for the depleted mid-ocean-ridge basalt mantle (DMM) are from Wang et al. (2017) and Sossi et al. (2018), Zn data are from McDonough and Sun (1995), Sr, Nd data and Sr–Nd isotope data are from Workman and Hart (2005).

[2]Zn isotope data for the normal mantle are from Wang et al. (2017), Mg isotope data are from Teng et al. (2010).

[3]Zn isotope data for silicate are from Frédéric et al. (2017) and references therein, Sr, Nd, Zn data and Sr–Nd isotope data are from Cousens et al. (1994).

[4]Zn isotope data for magnesite are from Pichat et al. (2003), Zn data are from Li et al. (2014), Sr data and Sr isotope data are from Huang and Xiao (2016), Nd data and Nd isotope data are from Demeny et al. (2004).

[5]Zn isotope data for dolomite are from Pichat et al. (2003), Zn data are from Li et al. (2014), Sr data and Sr isotope data for dolomite are from Huang and Xiao (2016).

[6]Compositions of the carbonated peridotites are represented by the Cenozoic nephelinites in eastern China, because they are the least influenced by the interaction with the lithosphere (Li and Wang, 2018; Wang et al., 2018). Melts derived from carbonated peridotites can be different in the compositions of trace elements (Dasgupta et al., 2007; Dasgupta et al., 2013). Carbonated silicate melts represent the

melting product of carbonated peridotites under low pressure, which involved in the interaction with mantle (Fig. 2B; Spera and Bohrson, 2001; Dasgupta et al., 2013). Trace elements and Zn–Sr–Nd isotope data for carbonated peridotites (carbonated silicate melts) are represented by Cenozoic Shandong nephelinites. Data for the Cenozoic Shandong alkaline igneous rocks are from Wang et al. (2018) and Zeng et al. (2010, 2011). Mg isotope data for carbonated peridotites are represented by the mantle xenoliths (wehrlites) in eastern China, which are from Xiao et al. (2013) and Su et al. (2019).

SUPPLEMENTARY REFERENCES

Andersen, T., 2002, Correction of common lead in U–Pb analyses that do not report 204 Pb: Chemical Geology, v. 192, p. 59-79.

Baker, J., Peate, D., Waight, T., and Meyzen, C., 2004, Pb isotopic analysis of standards and samples using a ^{207}Pb-^{204}Pb double spike and thallium to correct for mass bias with a double-focusing MC-ICP-MS: Chemical Geology, v. 211, p. 275–303, doi: 10.1016/j.chemgeo.2004.06.030.

Bao, Z.A., Huang, K.J., Huang, T.Z., Shen, B., Zong, C.L., Chen, K.Y., and Yuan, H.L., 2019, Precise magnesium isotope analyses of high-K and low-Mg rocks by MC-ICP-MS: Journal of Analytical Atomic Spectrometry, v. 34(5), p. 940-953, doi: 10.1039/C9JA00002J.

Bao, Z.A., Huang, K.J., Xu, J., Deng, Li., Yang, S.F., Zhang, P., and Yuan, H.L., 2020, Preparation and characterization of a new reference standard GSB-Mg for Mg isotopic analysis: Journal of Analytical Atomic Spectrometry, v. 35(6), p. 1080-1086, doi: 10.1039/d0ja00059k.

Chen, S., Liu, Y.C., Hu, J.Y., Zhang, Z.F., Hou, Z.H., Huang, F. and Yu, H.M., 2016, Zinc Isotopic Compositions of NIST SRM 683 and Whole-Rock Reference Materials: Geostandards and Geoanalytical Research, v. 40, p. 417-432, doi: 10.1111/j.1751-908X.2015.00377.x.

Cousens, B.L., 1994, Subduction-modified pelagic sediments as the enriched component in back-arc basalts from the Japan Sea: ocean drilling program sites 797 and 794: Contrib. Mineral. Petrol., v. 117(4), p. 421-434, doi: 10.1007/BF00307275.

Cruz-Uribe, A.M., Marschall, H.R., Gaetani, G.A., Le Roux, V., and Ronique, 2018, Generation of alkaline magmas in subduction zones by partial melting of

m élange diapirs_An experimental study: Geology, v. 46(4), p. 343-346, doi: 10.1130/G39956.1.

Dalton, J.A., and Wood, B.J., 1993, The compositions of primary carbonate melts and their evolution through wallrock reaction in the mantle: Earth Planet Sci Lett, v. 119, p. 511-525, doi: 10.1016/0012-821X(93)90059-I.

Dasgupta, R., Hirschmann, M.M., and Smith, N.D., 2007, Partial meltingexperiments of peridotite + CO_2 at 3 GPa and genesis of Alkalic Ocean Island Basalts: Journal of Petrology, v. 48, p. 2093-2124.

Dasgupta, R., Mallik, A., Tsuno, K., Withers, A.C., Hirth, G., and Hirschmann, M.M., 2013, Carbon-dioxide-rich silicate melt in the Earth's upper mantle: Nature, v. 493, p. 211-215, doi: 10.1038/nature11731.

Demeny, A., Vennemann, T.W., Hegner, E., Nagy, G., Milton, J.A., Embey-Isztin, A., Homonnay, Z., and Dobosi, G., 2004, Trace element and C-O-Sr-Nd isotope evidence for subduction-related carbonate-silicate melts in mantle xenoliths (Pannonian Basin, Hungary): LITHOS, v. 75(1), p. 89-113.

Depaolo, D.J., 1981, Trace element and isotopic effects of combined wall rock assimilation and fractional crystallization: Earth and Planetary Science Letters, v. 53, p. 189-202, doi: 10.1016/0012-821X(81)90153-9.

Dong, Y., Xiong S., Wang F., Ji, Z., Li, Y.B., Shinji, Y., Kiyoaki, N., and Xu, W.L., 2023, Triggering of episodic back-arc extensions in the northeast Asian continental margin by deep mantle flow: Geology, v. 51, p. 193-198, doi: 10.1130/G50724.1.

Fr édéric, M., Derek, V., Toshiyuki, F., and Paul, S., 2017, The isotope geochemistry of zinc and copper (Review): Reviews in Mineralogy and Geochemistry, v. 82(1), p. 543-600, doi: 10.2138/rmg.2017.82.13.

Galy, A., 2003, Magnesium isotope heterogeneity of the isotopic standard SRM980 and new reference materials for magnesium-isotope-ratio measurements: Journal of Analytical Atomic Spectrometry, v. 18(11), p. 1352-1356, doi: 10.1039/b309273a.

He, Y., Chen, L.H., Shi, J.H., Zeng, G., Wang, X.J., and Xue, X.Q., 2019, Light Mg isotopic composition in the mantle beyond the Big Mantle Wedge beneath eastern Asia: Journal of Geophysical Research: Solid Earth, v. 124, p. 8043-8056, doi: 10.1029/2018JB016857.

Huang, J., and Xiao, Y.L., 2016, Mg-Sr isotopes of low-delta ^{26}Mg basalts tracing recycled carbonate species: Implication for the initial melting depth of the carbonated mantle in Eastern China: International Geology Review, v. 58(11), p. 1350-1362, doi: 10.1080/00206814.2016.1157709.

Kuritani, T., Kimura, J., Ohtani, E., Miyamoto, H., and Furuyama, K., 2013, Transition zone origin of potassic basalts from Wudalianchi volcano, northeast China: Lithos, v. 156, p. 1-12, doi: 10.1016/j.lithos.2012.10.010.

Li, C.F., Li, X.H., Li, Q.L., Guo, J.H., Li, X.H., and Y ang, Y.H., 2012, Rapid and precise determination of Sr and Nd isotopic ratios in geological samples from the same filament loading by thermal ionization mass spectrometry employing a single-step separation scheme: Analytica Chimica Acta, v. 727, p. 54-60, doi: 10.1016/j.aca.2012.03.040.

Li, J., Tang, S.H., Zhu, X.K., and Pan, C.X., 2017, Production and Certification of the Reference Material GSB 04-3258-2015 as a ^{143}Nd/^{144}Nd Isotope Ratio Reference: Geostandards and Geoanalytical Research, v. 41(2), p. 255-262, doi: 10.1111/ggr.12151.

Li, J.L., Klemd, R., Gao, J., and Meyer, M., 2014, Compositional zoning in dolomite

from lawsonite-bearing eclogite (SW Tianshan, China): Evidence for prograde metamorphism during subduction of oceanic crust: American Mineralogist, v. 99(1), p. 206-217, doi: 10.2138/am.2014.4507.

Li, S.G., and Wang, Y., 2018, Formation time of the big mantle wedge beneath eastern China and a new lithospheric thinning mechanism of the North China Craton—Geodynamic effects of deep recycled carbon: Scientia Sinica (Terrae), v. 7, p. 809-824, doi: 10.1007/s11430-017-9217-7.

Li, X.H., Liu, Y., Li, Q.L., Guo, C.H., and Chamberlain, K.R., 2009, Precise determination of Phanerozoic zircon Pb/Pb age by multicollector SIMS without external standardization: John Wiley & Sons, Ltd.

Lin, J., Liu, Y., Y ang, Y., and Hu, Z., 2016, Calibration and correction of LA-ICP-MS and LA-MC-ICP-MS analyses for element contents and isotopic ratios: Solid Earth Sciences, v. 1, p. 5-27, doi: 10.1016/j.sesci.2016.04.002.

Liu, Y., Gao, S., Hu, Z., Gao, C., Zong, K., and Wang, D., 2010, Continental and Oceanic Crust Recycling-induced Melt–Peridotite Interactions in the Trans-North China Orogen: U–Pb Dating, Hf Isotopes and Trace Elements in Zircons from Mantle Xenoliths: Journal of Petrology, p. 392-9.

Liu, Y., Hu, Z., Gao, S., Günther, D., and Xu, J., 2008, In situ analysis of major and trace elements of anhydrous minerals by LA-ICP-MS without applying an internal standard: Chemical Geology, v. 257, p. 34-43.

Ludwig, K.R., 2003, ISOPLOT 3.0: A Geochronological Toolkit for Microsoft Excel. Berkeley Geochronology Center Special Publication.

McDonough, W.F., and Sun, S.S., 1995, The composition of the Earth: Chemical Geology, v. 120(3), p. 223-253, doi: 10.1016/0009-2541(94) 00140-4.

Nielsen, S.G., and Marschall, H.R., 2017, Geochemical evidence for mélange melting

in global arcs: Science Advances, v. 3(4), doi: 10.1126/sciadv.1602402.

Pichat, S., Douchet, C., and Albarède, F., 2003, Zinc isotope variations in deep-sea carbonates from the eastern equatorial Pacific over the last 175 ka: Earth and Planetary Science Letters, v. 210, p. 167, doi: 10.1016/S0012-821X(03)001067.

Russell, W.A., Papanastassiou, D.A., and Tombrello, T.A., 1978, Ca isotope fractionation on the Earth and other solar system materials: Geochimica et Cosmochimica Acta, v. 42, p. 1075-1090, doi: 10.1016/0016-7037(78)90105-9.

Sossi, P.A., Nebel, O., O'Neill, H.S., and Moynier, F., 2018, Zinc isotope composition of the Earth and its behaviour during planetary accretion: Chemical Geology, v. 477, p. 73-84, doi: 10.1016/j.chemgeo.2017.12.006.

Spera, F.J., Bohrson, W.A., 2001, Energy-Constrained Open-System Magmatic Processes I: General Model and Energy-Constrained Assimilation and Fractional Crystallization (EC-AFC) Formulation: Journal of Petrology, v. 42(5), p. 999-1018, doi: 10.1093/petrology/42.5.999.

Stacey, J.S., and Kramers, J.D., 1975, Approximation of terrestrial lead isotope evolution by a two-stage model: Earth and Planetary Science Letters, v. 26, p. 207-221, doi: 10.1016/0012-821X(75)90088-6.

Su, B.X., Hu, Y., Teng, F.Z., Xiao, Y., Zhang, H.F., Sun, Y., Bai, Y., Zhu, B., Zhou, X.H., and Ying, J.F., 2019, Light Mg isotopes in mantle-derived lavas caused by chromite crystallization, instead of carbonatite metasomatism: Earth and Planetary Science Letters, v. 522, p. 79-86, doi: 10.1016/j.epsl.2019.06.016.

Teng, F.Z., 2017, Magnesium Isotope Geochemistry: Reviews in Mineralogy and Geochemistry, v. 82(1), p. 219-287, doi: 10.2138/rmg.2017.82.7.

Teng, F.Z., Li, W.Y., Ke, S., Marty, B., Dauphas, N., Huang, S., Wu, F.Y., and Pourmand, A., 2010, Magnesium isotopic composition of the Earth and chondrites: Geochim Cosmochim Acta, v. 74, p. 4150–4166, doi: 10.1016/j.gca.2010.04.019.

Thirlwall, M.F., 1991, Long-term reproducibility of multicollector Sr and Nd isotope ratio analysis: Chemical Geology, v. 94(2), p. 85-104, doi: 10.1016/S0009-2541(10)80021-X.

Wang, K., Cai, K.D., Sun, M., Wang, X.S., Xia, X.P., Zhang, B., and Wan, B., 2022, Diapir Melting of Subducted Mélange Generating Alkaline Arc Magmatism and Its Implications for Material Recycling at Subduction Zone Settings: Geophysical Research Letters, v.49(10), p. 1-13, doi: 10.1029/2021 GL097693.

Wang, Z.Z., Liu, S.A., Chen, L.H., Li, S.G., and Zeng, G., 2018, Compositional transition in natural alkaline lavas through silica-undersaturated melt-lithosphere interaction: Geology, v. 46, p. 771-774, doi: 10.1130/G45145.1.

Wang, Z.Z., Liu, S.A., Liu, J.G., Huang, J., Xiao, Y., Chu, Z.Y., Zhao, X.M., and Tang, L.M., 2017, Zinc isotope fractionation during mantle melting and constraints on the Zn isotope composition of Earth's upper mantle: Geochimica et Cosmochimica Acta, v. 198(1), p. 151-167, doi: 10.1016/j.gca.2016.11.014.

Weis, D., Kieffer, B., Maerschalk, C., Barling, J., Jong, J.D., Williams, G.A., Hanano, D., Pretorius, W., Mattielli, N., Scoates, J.S., Goolaerts, A., Friedman, R.M., and Mahoney, J.B., 2006, High-precision isotopic characterization of USGS reference materials by TIMS and MC-ICP-MS: G-Cubed: Geochemistry, Geophysics, Geosystems: an electronic journal of the Earth sciences, v .7(8), p. Q08006, doi: 10.1029/2006GC001283.

Wiedenbeck, M., Allé, P., Corfu, F., Griffin, W. L., Meier, M., Oberli, F., Quadt, A.V., Roddick, J. c., and Spiegel, W., 1995, Three Natural Zircon Standards for U-Th-Pb, Lu-Hf, Trace Element and Ree Analyses: Geostandards Newsletter, v. 19, p. 1-23, doi: 10.1111/j.1751-908X.1995.tb00147.x.

Workman, R.L., and Hart, S.R., 2005, Major and trace element composition of the depleted MORB mantle (DMM): Earth and Planetary Science Letters, v. 231, p. 53-72, doi: 10.1016/j.epsl.2004.12.005.

Xiao, Y., Teng, F.Z., Zhang, H.F., Yang, W., 2013, Large magnesium isotope fractionation in peridotite xenoliths from eastern North China craton: Product of melt–rock interaction: Geochimica et Cosmochimica Acta, v.115(1), p. 241-261, doi: 10.1016/j.gca.2013.04.011.

Yuan, H., Gao, S., Liu, X., Li, H., Günther, D., and Wu, F., 2004, Accurate U-Pb Age and Trace Element Determinations of Zircon by Laser Ablation- Inductively Coupled Plasma-Mass Spectrometry: Geostandards and Geoanalytical Research, v. 28, p. 353-370, doi: 10.1111/j.1751-908X.2004.tb00755.x.

Zeng, G., Chen, L.H., Hofmann, A., Jiang, S.Y., and Xu, X.S., 2011, Crust recycling in the sources of two parallel volcanic chains in Shandong, North China: Earth and Planetary Science Letters, v. 3, p. 359-368, doi: 10.1016 /j.epsl.2010.12.026.

Zeng, G., Chen, L.H., Xu, X.S., Jiang, S.Y., and Hofmann, A.W., 2010, Carbonated mantle sources for Cenozoic intraplate alkaline basalts in Shandong, North China: Chemical Geology, v. 273, p. 35-45, doi: 10.1016/j.chemgeo.2010.02.009.

Zhang, W., Hu, Z.C., and Liu, Y.S., 2020, Iso-Compass: new freeware software for isotopic data reduction of LA-MC-ICP-MS: Journal of Analytical Atomic

Spectrometry, v. 35(6), p. 1087-1096, doi: 10.1039/D0JA00084A.

Zhu, Y.T., Li, M., Wang, Z.C., Zou, Z.Q., Hu, Z.C., Liu, Y.S., Zhou, L., and Chai, X.N., 2019, High-precision copper and zinc isotopic measurements of igneous rock standards using a large-geometry MC-ICP-MS: Atomic spectroscopy, v. 40(6), p. 206-214.